

Current spin polarization of a platform molecule with compression effect

Zhi Yang(羊志)1, Feng Sun(孙峰)1, Deng-Hui Chen(陈登辉)1, Zi-Qun Wang(王子群)2, Chuan-Kui Wang(王传奎)1, Zong-Liang Li(李宗良)1,†, and Shuai Qiu(邱帅)1,‡

Citation: Chin. Phys. B, 2022, 31 (7): 077202 DOI: 10.1088/1674-1056/ /ac4f53
Journal homepage: http://cpb.iphy.ac.cn; http://iopscience.iop.org/cpb

What follows is a list of articles you may be interested in

Theoretical design of thermal spin molecular logic gates by using a combinational molecular junction

Yi Guo(郭逸), Peng Zhao(赵朋), and Gang Chen(陈刚)
Chin. Phys. B, 2022, 31 (**4**): 047202. DOI: 10.1088/1674-1056/ac3a5f

Separating spins by dwell time of electrons across parallel double *δ*-magnetic-barrier nanostructure applied by bias

Sai-Yan Chen(陈赛艳), Mao-Wang Lu(卢卯旺), and Xue-Li Cao(曹雪丽)
Chin. Phys. B, 2022, 31 (**1**): 017201. DOI: 10.1088/1674-1056/abeb09

Recent spinterfacial studies targeted to spin manipulation in molecular spintronic devices

Xian-Rong Gu(谷现荣), Li-Dan Guo(郭立丹), Xiang-Nan Sun(孙向南)
Chin. Phys. B, 2018, 27 (**10**): 107202. DOI: 10.1088/1674-1056/27/10/107202

Thermal stability of the spin injection in Co/Ag/Co lateral spin valves

Le Wang(王乐), Lu-Chen Chen(陈鹭琛), Wen-Yu Liu(刘雯雨), Shuo Han(韩烁), Weiwei Wang(王伟伟), Zhanjie Lu(卢占杰), Shan-Shan Chen(陈珊珊)
Chin. Phys. B, 2018, 27 (**9**): 097202. DOI: 10.1088/1674-1056/27/9/097202

A spin switch device based on a triple quantum dots superlattice using the Dicke effect

An Xing-Tao, Mu Hui-Ying, Xian Li-Fen, Liu Jian-Jun
Chin. Phys. B, 2012, 21 (**7**): 077201. DOI: 10.1088/1674-1056/21/7/077201

Current spin polarization of a platform molecule with compression effect

Zhi Yang(羊志)[1], Feng Sun(孙峰)[1], Deng-Hui Chen(陈登辉)[1], Zi-Qun Wang(王子群)[2], Chuan-Kui Wang(王传奎)[1], Zong-Liang Li(李宗良)[1,†], and Shuai Qiu(邱帅)[1,‡]

[1] *Shandong Key Laboratory of Medical Physics and Image Processing & Shandong Provincial Engineering and Technical Center of Light Manipulations, School of Physics and Electronics, Shandong Normal University, Jinan* 250358, *China*

[2] *Zao Zhuang University, Zao Zhuang* 277160, *China*

(Received 16 December 2021; revised manuscript received 13 January 2022; accepted manuscript online 27 January 2022)

Using the first-principles method, the spin-dependent transport properties of a novel platform molecule containing a freestanding molecular wire is investigated by simulating the spin-polarized scanning tunneling microscope experiment with Ni tip and Au substrate electrodes. Transport calculations show that the total current increases as the tip gradually approaches to the substrate, which is consistent with the conductance obtained from previous experiment. More interestingly, the spin polarization (SP) of current modulated by compression effect has the completely opposite trend to the total current. Transmission analyses reveal that the reduction of SP of current with compression process originates from the promotion of spin-down electron channel, which is controlled by deforming the molecule wire. In addition, the density of states shows that the SP of current is directly affected by the organic–ferromagnetic spinterface. The weak orbital hybridization between the Ni tip and propynyl of molecule results in high interfacial SP, whereas the breaking of the C≡C triple of propynyl in favor of the Ni–C–C bond induces the strong orbital hybridization and restrains the interfacial SP. This work proposes a new way to control and design the SP of current through organic–ferromagnetic spinterface using functional molecular platform.

Keywords: molecular spintronics, spin-dependent transport, spin polarization, single-molecule junctions

PACS: 72.25.–b, 75.47.–m, 85.75.–d **DOI:** 10.1088/1674-1056/ac4f53

1. Introduction

Molecular spintronics is a fascinating and frontier subfield of spintronics, which focuses on the spin degrees of freedom of electrons based on organic molecules.[1–5] Organic molecules exhibit the advantages of weak spin–orbit coupling and long spin relaxation times, which is conductive to spin transport and manipulation.[6,7] More importantly, when organic molecules contact the ferromagnetic metals to form a spinterface, the hybrid interface states (HIS) can be generated from the orbital hybridization between molecules and ferromagnets.[8–11] The HIS usually appears near the Fermi level, which determines the spin injection efficiency and transport property.[12] Moreover, comparing with the original ferromagnetic metal, enhancement or reversal of interfacial spin polarization (SP) can be observed to be attributed to HIS.[13–15] A lot of researches have demonstrated the crucial effect of HIS on spin-dependent transport properties in magnetic single-molecule junctions.[16–19]

As various novel molecules are designed and synthesized, a series of molecular spintronic devices is engineered and extensively investigated in theory and experiment , such as spin filter,[20–22] spin rectifier,[23,24] spin transistors,[25,26] and spin logic gates.[27,28] Thus, it is of utmost importance to search for specific functional molecules for developing molecular spintronic devices. Recently, the extended aromatic platform molecules have attracted much attention of researchers. Since the platform of molecule contacts the substrate electrode flatly via physisorption instead of chemisorption, the conductance of molecular junction is mediated by the electronic coupling between the tip electrode and the freestanding molecular wire.[29,30] In 2017, Jasper-Tönnies *et al.* investigated the conductance properties of propynyl–trioxatriangulenium (P-TOTA) molecular junction by using the scanning tunneling microscope with Au tip and substrate electrodes under compression process. The conductance is related to the deformation of molecule wire, where the bonding way between Au tip and molecule as well as the symmetry mismatch of Au atoms and molecule orbitals plays a key role.[29] Then, they further investigated the conductance of similar platform molecule by replacing propynyl in P-TOTA molecule with hydrogen or methyl,[31] where the excellent charge transport performance of platform molecular junction is widely validated.[32,33] However, the spin-dependent transport properties of platform molecule have not been studied so far. Considering that the spinterface formed between the propynyl of P-TOTA molecule and the top electrode must be changed with the deformation of propynyl in the compression process, the spin transport of P-TOTA magnetic molecular junction modu-

†Corresponding author. E-mail: lizongliang@sdnu.edu.cn
‡Corresponding author. E-mail: shuaiqiu@sdnu.edu.cn

© 2022 Chinese Physical Society and IOP Publishing Ltd

lated by the HIS is an issue worth exploring. Therefore, there is an enormous significance in promoting the applications of P-TOTA molecule in molecular spintronics.

In this work, the response of spin-dependent transport properties of P-TOTA magnetic molecular junctions to the compression effect is theoretically investigated. We adopt the ferromagnetic Ni tip electrode and non-magnetic Au substrate electrode to simulate the spin-polarized scanning tunneling microscope (SP-STM) experiment. The results demonstrate that the current and SP of current have completely opposite trends with the change of compression effect under bias voltage, which is due to the fact that the spin transport is controlled by the HIS. The mechanism of orbital hybridization between Ni electrode and propynyl of P-TOTA molecule is elucidated, which is responsible for the SP of current. In the rest of this work is organized as follows. The theoretical model and computational details are introduced in Section 2. The results and discussion are analysed in Section 3. The conclusion is finally summarized in Section 4.

2. Theoretical model and computational details

The theoretical models of magnetic single-molecule junctions are presented in Fig. 1. A P-TOTA molecule is absorbed on the non-magnetic Au (111) bottom electrode with 6×6 unit cell periodicity. The ferromagnetic Ni (111) top electrode with a ten-atom tetrahedron is used as the tip of the SP-STM. To simulate the compression process of this molecular junction, the tip of SP-STM slides toward the substrate and three schematic structures are obtained as displayed in Fig. 1. For the initial configuration M1, the distance between top electrode and bottom electrode is 11.3 Å and the propynyl of P-TOTA molecule keeps upright. When the top electrode is close to the bottom electrode, the interaction between propynyl and tip is gradually enhanced. As the distance between the two electrodes decreases to 9.5 Å, the propynyl bends 160° and configuration M2 is obtained as shown in Fig. 1(b). When we move the top electrode further down to 7.3 Å, the propynyl is bent more seriously. As displayed in Fig. 1(c), the angle of propynyl is 148° for the final configuration M3. Furthermore, two carbon atoms of propynyl are bonded to the tip atom of Ni electrode, which breaks an original C≡C triple band and forms a new Ni–C–C bond. We calculate the total energy of the three optimized configurations, where is −300988.35 eV, −300988.70 eV, and −300990.86 eV for M1, M2, and M3 junctions, respectively. It is clearly seen that the structure is more stable in the compression process. The difference in total energy between M1 and M2 junctions is only 0.35 eV, whereas that between M2 and M3 junctions is 2.16 eV. Apparently, from M1 to M2 junction, the weak interaction between Ni tip electrode and propynyl of P-TOTA molecule induces a small energy difference. However, when M2 junction is further compressed to obtain M3 junction, the breaking and forming of chemical bonds lead the energy to decrease significantly.

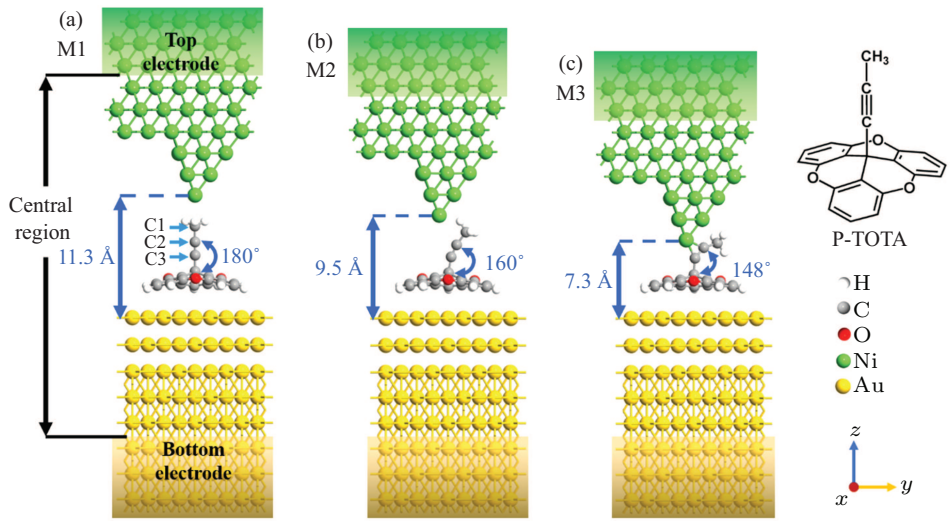


Fig. 1. Schematic diagrams of compression processes about P-TOTA molecular junction for three structures: (a) M1, (b) M2, and (c) M3. The carbon atoms of propynyl of P-TOTA molecule are marked from top to bottom with C1, C2, and C3, respectively. The white, gray, red, green and yellow balls denote H, C, O, Ni, and Au atoms, respectively.

The geometry optimization of the P-TOTA molecule and three device configurations are calculated based on density functional theory (DFT), where the maximum residual force on each atom is less than 0.04 eV/Å. The spin-dependent electron transport properties are further investigated by combining the DFT with non-equilibrium Green's function (NEGF) method[34] implemented in Atomistix ToolKit (ATK) package.[35,36] Firstly, the isolated P-TOTA molecule is optimized. Then, the optimized molecule is placed between two electrodes to simulate the compression process, forming three central regions. The central region composed of optimized molecule and five layers of Au electrodes and six layers of

Ni electrodes is further optimized. In this process, the atoms of Ni tetrahedral tip and the two innermost layers atoms of Au slab are completely optimized, while the rest of Ni atoms are fixed, and the remaining Au atoms are restricted to move rigidly. In order to choose appropriate lattice structures of two different electrodes, based on the matching algorithm, the two electrode structures are evaluated and the mismatch between the lattice constants is 0.07%. In the whole calculations, the spin-polarized generalized gradient approximation (SGGA) with the Perdew–Burke–Ernzerhof (PBE)[37] is used as the exchange–correlation functional. The Troullier–Martins type norm-conserving pseudopotentials[38] are adopted. The K-point sampling is $3\times3\times100$ in each of the x, y, and z directions, where the z direction is the electron transport direction. The density mesh cutoff for real space grids is set to be 200 Ry (1 Ry = 13.6056923(12) eV), and the tolerance convergence in the self-consistent loop is less than 1.0×10^{-4} Hartree (1 Hartree = 4.3597×10^{-18} J). The double zeta (ζ) polarization (DZP) basis set is used for hydrogen, carbon, and oxygen atoms, as well as the single zeta (ζ) polarization (SZP) basis set is applied to Ni and Au atoms to make a balance between computational accuracy and computational quantity.[39,40] A positive bias voltage is applied to the Ni electrode, and a negative bias voltage to the Au electrode.

The spin-polarized current I under a bias voltage V is calculated from the Landauer–Büttiker formula[41]

$$I_\sigma = \frac{e}{h}\int T_\sigma(E,V)[f_{\rm T}(E-\mu_{\rm T}) - f_{\rm B}(E-\mu_{\rm B})]\,{\rm d}E. \quad (1)$$

In formula (1), σ is the spin orientation (spin-up or spin-down) of the electrons, e represents the elementary electron charge, h denotes the Planck's constant, $f_{\rm T}(E-\mu_{\rm T})$ and $f_{\rm B}(E-\mu_{\rm B})$ are the Fermi–Dirac distribution functions for electrons in the top electrode and the bottom electrode, respectively, and $\mu_{\rm T}$ and $\mu_{\rm B}$ are the the electrochemical potentials of top electrode and bottom electrode, and $T_\sigma(E,V)$ is the spin-dependent transmission spectrum, and expressed as

$$T_\sigma(E,V) = {\rm Tr}[\Gamma_{\rm T}(E,V)G_{\rm C}(E,V)\Gamma_{\rm B}(E,V)G_{\rm C}^{+}(E,V)]. \quad (2)$$

In formula (2), $G_{\rm C}(E,V)$ is Green's function of the central region, $\Gamma_{\rm T}(E,V)$ denotes the coupling matrix between the central scattering region and the top electrode, and $\Gamma_{\rm B}(E,V)$ refers to the matrix between the central scattering region and the bottom electrode.

3. Results and discussion

In the previous STM experiment, the conductance of the P-TOTA molecular junction using Au tip and substrate electrodes gradually increased with the interelectrode distance decreasing.[29] Herein, we replace the Au tip with Ni tip. And we first investigate the spin-dependent transport properties of P-TOTA molecule changing with the compression effect. The total current–voltage (I–V) curves and the SP of current of M1–M3 junctions are calculated under the bias voltage varying from 0.0 V to 0.5 V with a bias step of 0.1 V as shown in Fig. 2. It is clearly seen that the total currents of the three molecular junctions are all increasing with the bias voltage increasing. The current of M1 junction and M2 junction are extremely close to each other and each maintains a very low level, where the maximum value is only about 50 nA and 20 nA at 0.5 V, respectively. However, for M3 junction, the current has a significant enhancement, where the maximum value reaches about 750 nA at 0.5 V. More importantly, the maximum values of total currents increase in the order of M1<M2<M3 obtained in the compression process, which conforms to the results from previous STM experiment. The SP of current is calculated as follows: $SP(V) = \left[I_\uparrow(V) - I_\downarrow(V)\right] / \left[I_\uparrow(V) + I_\downarrow(V)\right] \times 100\%$, where $I_\uparrow(V)$ and $I_\downarrow(V)$ are the spin-up current and spin-down current, respectively. As depicted in Fig. 2(b), for M1 junction, the SP of current increases with bias voltage rising, where the maximum value is about 45% near 0.5 V. The variation tendency of M2 junction is similar to that of M1 junction, where the maximum value reaches only 25% at 0.4 V. However, for M3 configuration, the SP of current decreases from 18% to 6% under calculated bias voltage. Interestingly, it is found that the SP of current always decreases with the diminution of interelectrode distance, which displays opposite variation trend compared with that of current. Moreover, the SP of current shows three different intensities with the change of bias voltage. Therefore, the spin transport properties of P-TOTA molecule in SP-STM have a significant response to the compression effect.

To explain the spin transport properties of P-TOTA molecule, we calculate the spin-dependent transmission spectra of M1, M2, and M3 junction under 0.0 V and 0.4 V, respectively. The transmission spectra are plotted in logarithmic coordinates to obtain a more intuitive view as shown in Fig. 3. The eigenvalues of spin-dependent molecular-projected self-consistent Hamiltonian (MPSH)[42] are also marked to distinguish between molecular orbitals and HIS. It is evidently seen that the transmission coefficients of M1, M2, and M3 junction near the Fermi level all increase by an order of magnitude with interelectrode distance shortening under 0.0 V and 0.4 V, which accounts for the results of the total current in Fig. 2(a). Besides, the spin-up transmission coefficients of the three junctions are larger than the spin-down ones, which leads to the spin-up SP of current. For M1 and M2 junction shown in Figs. 3(a), 3(b), 3(d), and 3(e), two spin-up peaks appear near the Fermi level, which has no MPSH eigenvalues corresponding to them. This indicates that they are not the molec-

ular orbits caused by the self-energy of the electrode, but are the HIS generated by the interface hybridization. The spin-up HIS transmission peaks move toward higher energy and enter into the bias window with the increase of bias voltage, which brings about the enhancement of SP of current. Moreover, the spin-up HIS transmission peak of M1 junction in the bias window is wider than that of M2 junction, which gives rise to larger SP of current than that of M2 junction. However, in Figs. 3(c) and 3(f), the transmission peaks contributed by the molecular orbits appear near the Fermi level, which causes a huge current for M3 junction. The spin-up transmission coefficient and the spin-down transmission coefficient of M3 junction in the bias window have the same magnitudes, which results in minimum SP of current for the three junctions.

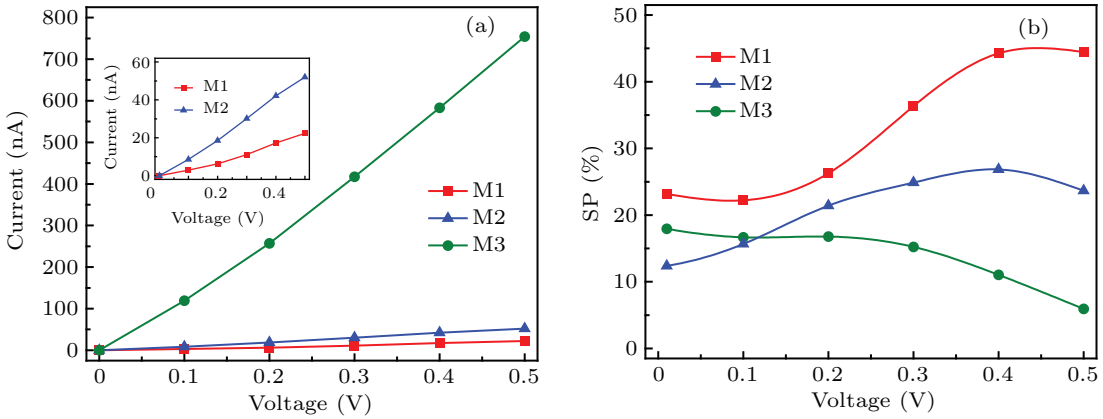


Fig. 2. (a) Total current–voltage curves and (b) bias-dependent SP of current of M1, M2, and M3 junctions. The inset in panel (a) shows the magnified part of plots of current–voltage curves for M1 and M2 junctions.

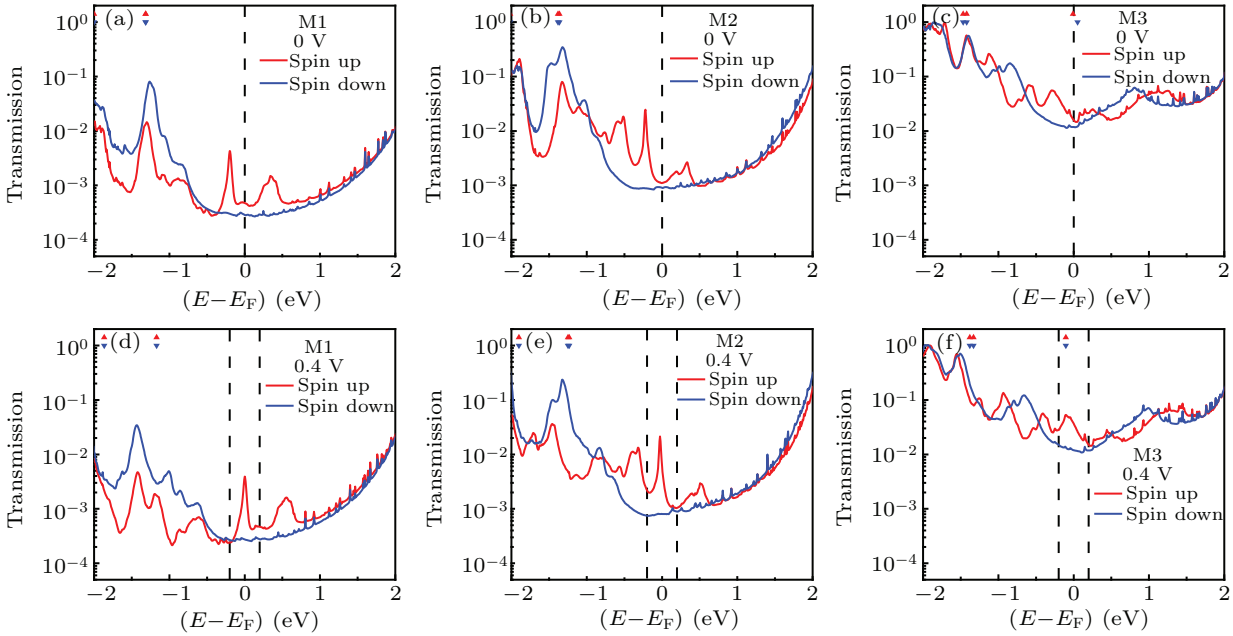


Fig. 3. Spin-dependent transmission spectra of M1, M2, and M3 junctions under ((a)–(c)) 0.0 V and ((d)–(f)) 0.4 V, respectively, where zero energy is Fermi level and the region between two dash lines indicates bias window. Red and blue triangles represent spin-up and spin-down MPSH eigenvalues, respectively.

To more intuitively analyze the transmission of electrons at bias voltage, the spin-dependent transmission pathways of the three junctions at Fermi level under 0.4 V are given in Fig. 4. The blue line and the red line between two atoms represent the pathway of transmission and the pathway of reflection, respectively. And the radius value of blue line and the red line represent the value of transmission probability and reflection probability, respectively. The thresholds are fixed at 0.0005 for all plots to compare different configurations. For all junctions, the extremely dense transmission and reflection pathways between Au substrate surface and platform of P-TOTA molecule are presented. Thus, the electron transport properties are mainly dependent on the interface between Ni tip and propynyl of P-TOTA molecule. For the M1 junction (as shown in Figs. 4(a) and 4(b)), the spin-up electrons can transport from the H atoms at the end of P-TOTA molecule to the Ni apex atom, but the spin-down electrons are suppressed. This induces the highest SP of current. For the M2 junction (as shown in Figs. 4(c) and 4(d)), the electrons can transport from the C2 atom of propynyl to the Ni apex atom. Although

the spin-down electrons have an additional transmission pathway from molecule to the Ni electrode, the radius magnitude of the spin-up transmission pathway from the C2 atom to the Ni apex atom is larger than that of spin-down one. Moreover, the platform of P-TOTA molecule provides more spin-up transmission pathways to C3 atom of propynyl. Therefore, the current of M2 junction is spin-up polarized and has a medium intensity in each of the three molecular junctions. For M3 junction, the spin-up transmission pathways are similar to the spin-down ones in the Ni-propynyl hybrid interface due to the strong chemical contact between Ni tip atom and C2 atom and between Ni tip atom and C3 atom of propynyl as shown in Figs. 4(e) and 4(f), respectively. However, the spin-up transmission pathways diffusely extend to the third layer of the Ni slab electrode, which is more delocalized than the spin-down ones and still leads to a smaller spin-up polarized current. Consequently, the results of spin-dependent transmission spectra and transmission pathways account for the change of SP of current in compressing process under higher bias.

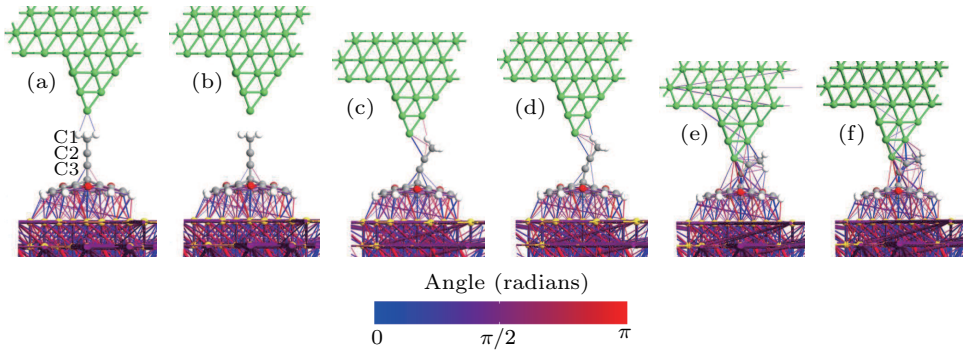


Fig. 4. Transmission pathways of three junctions at Fermi level under 0.4 V, showing [(a), (c), and (e)] spin-up electrons and [(b), (d), and (f)] spin-down electrons for M1, M2, and M3 junctions, respectively. Carbon atoms of propynyl are marked from top to bottom with C1, C2, and C3, respectively. Thresholds are fixed at 0.0005 for all plots.

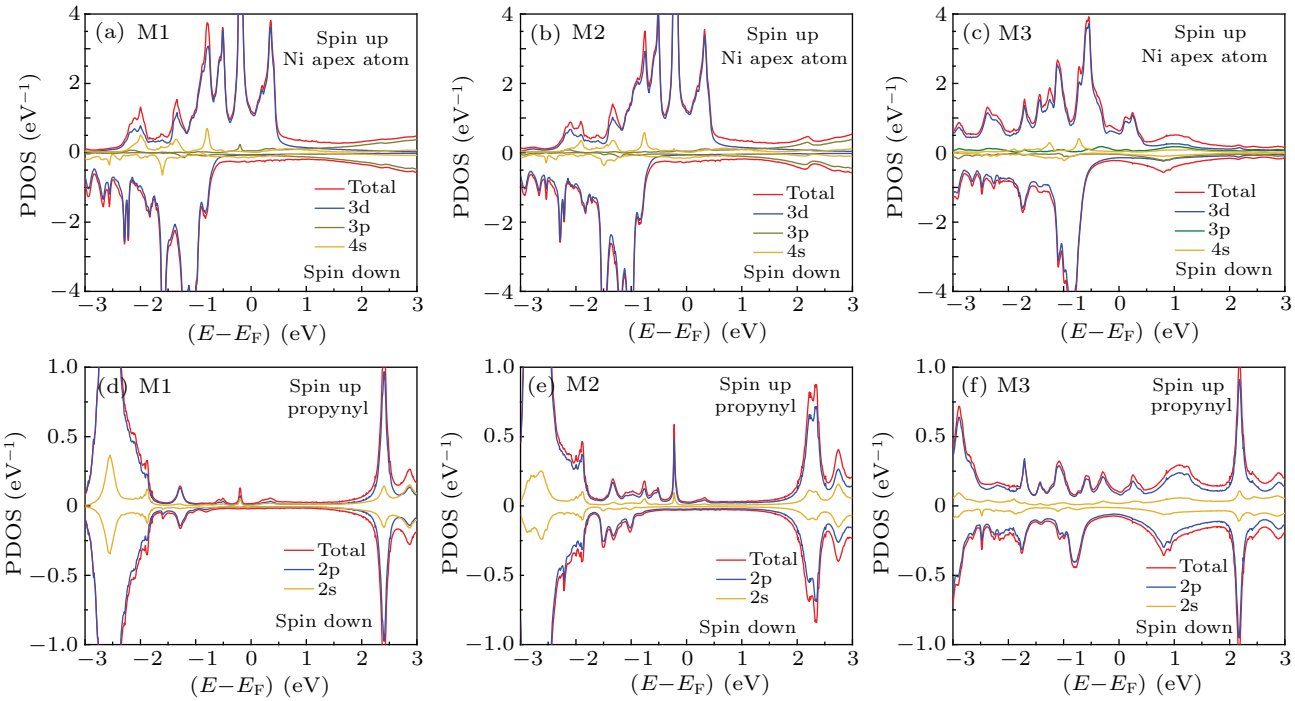


Fig. 5. Spin-dependent PDOS of Ni apex atom in (a) M1, (b) M2, and (c) M3 under zero bias voltage. And the spin-dependent PDOS of the propynyl of P-TOTA molecule in (d) M1, (e) M2, and (f) M3 under zero bias voltage.

Now, we turn to the spin-dependent transport mechanism affected by the Ni-propynyl hybrid interface. The spin-dependent projected density of states (PDOS) of the Ni apex atom and the propynyl of P-TOTA molecule in the three junctions under zero bias voltage are given in Fig. 5. Apparently, the PDOS peaks of the Ni apex atom and the propynyl near the Fermi level are mainly contributed by 3d orbitals and 2p orbitals, respectively. For M1 junction and M2 junction, the PDOS of the Ni apex atom is extremely similar, where they have many spin-up PDOS peaks near the Fermi level as indicated in Figs. 5(a) and 5(b). Meanwhile, there is a spin-up PDOS peak on each side of the Fermi level for propynyl (see

Figs. 5(d) and 5(e)), corresponding to the PDOS peak of the Ni apex atom, which indicates that the 3d orbital of Ni apex atom is hybridized with the propynyl. The PDOS peaks of the propynyl of M2 junction near the Fermi level are significantly strengthened compared with that of M1 junction, which reveals that the strength of orbital hybridization between Ni apex atom and propynyl increases evidently with the compression process going on. However, the spin-down PDOS of Ni apex atom and propynyl near the Fermi level are closely restrained, which results in the blocking of the spin-down channel and the spin-up polarization of the current. With the continuous compression of the molecular junction to M3, the C2 atom and C3 atom of propynyl contact the Ni apex atom, which causes the orbital hybridization of the Ni-propynyl interface to become more intense. Unlike the M1 junction and M2 junction, the PDOS of M3 junction changes obviously as shown in Figs. 5(c) and 5(f). Especially, the spin-down PDOS of the propynyl increases significantly near the Fermi level, which indicates that the spin-down channel is activated, leading the spin-up polarization of the current to decrease. Thus, the spin-dependent PDOS is affected by the change of organic–ferromagnetic interface originating from the compression process, which is responsible for the variation of spin-dependent transport.

In order to explore the contribution of every atom to the electronic states in the junction, the spatial distributions of local density of states (LDOS) for the energy of each spin-up PDOS peak of propynyl near the Fermi level under zero bias voltage are plotted in Fig. 6. It can be intuitively seen that the spin-up and spin-down LDOS are both distributed mainly in Ni electrode and partially exists in Au electrode, which indicates that the PDOS peaks of propynyl are contributed mainly by electrode atoms. For the M1 junction, the LDOS has almost no distribution on P-TOTA molecule (see Figs. 6(a), 6(b), 6(g), and 6(h)). However, with the decrease of the interelectrode distance, the interaction between Ni electrode and P-TOTA molecule is enhanced. The spin-up LDOS of M2 junction shown in Figs. 6(c) and 6(d) appears in methyl and C3 atom of propynyl, especially at the energy of −0.22 eV, where is attributed to a high PDOS peak shown in Fig. 5(e). But the spin-down LDOS of M2 junction shown in Figs. 6(i) and 6(j) is still similar to the LDOS of M1 junction. Being compressed futher, the C2 and C3 atoms of propynyl are bonded to the Ni apex atom. From Figs. 6(e), 6(f), 6(k), and 6(l), it is evidently seen that the spin-up LDOS and the spin-down LDOS increase in the three atoms, which testifies to the strong orbital hybridization between Ni apex atom and C2 and C3 atoms of propynyl. Note that the spin-down electronic states in M3 junction are distributed in the molecule, which means that the spin-down electronic channel is turned on with the compression process. Therefore, the compression process of P-TOTA molecular junction modifies the organic–ferromagnetic spinterface remarkably and dominates the electronic states for spin-dependent transport.

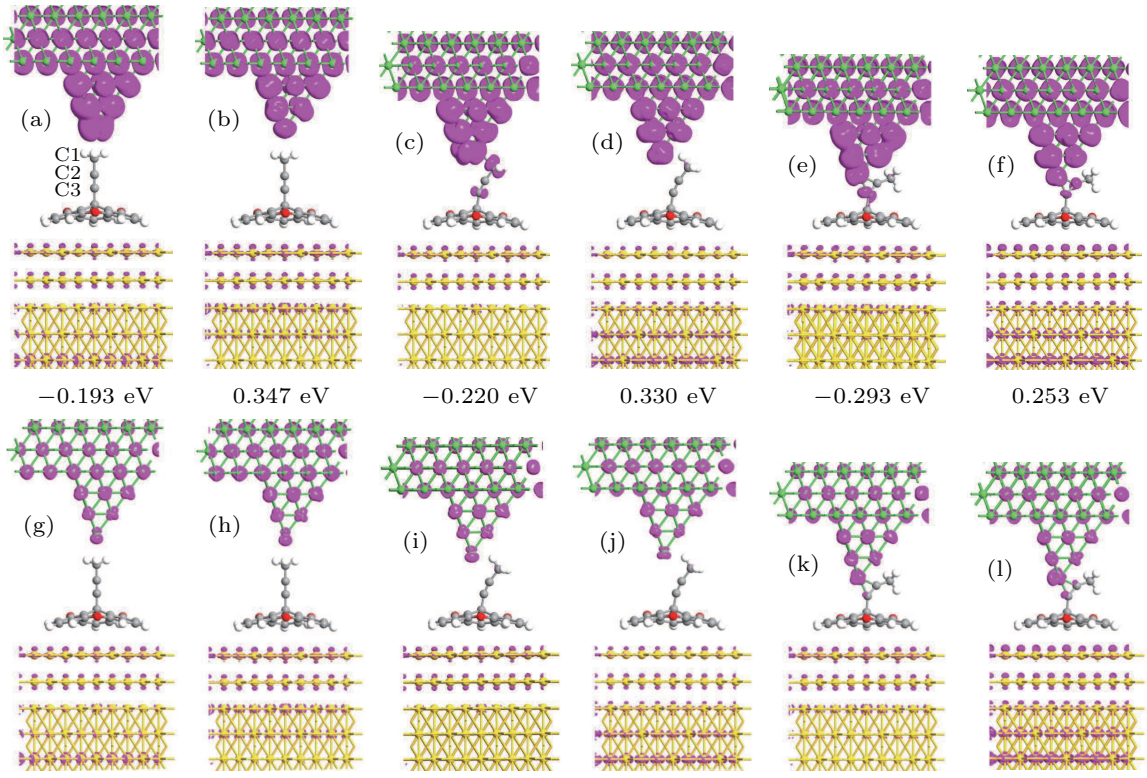


Fig. 6. Spin-up LDOS of [(a), (b)] M1, [(c), (d)] M2, and [(e), (f)] M3 junctions, and spin-down LDOS of [(g), (h)] M1, [(i), (j)] M2, and [(k), (l)] M3 junctions at certain energy under zero bias voltage. Carbon atoms of propynyl are marked from top to bottom with C1, C2, and C3, respectively. Isovalues are fixed at 0.03 for all isosurface plots.

4. Conclusions

In this work, according to the first-principles calculations of DFT combined with NEGF, we theoretically investigate the spin-dependent transport properties of P-TOTA molecule by simulating the compression process of SP-STM experiment with Ni tip electrode and Au substrate electrode. The computational results show that the current gradually increases with interelectrode distance shortening, which is coincident with that of conductance in previous STM experiment with Au electrode. However, it is extremely intriguing that the SP of current decreases with the compression process going on when the bias voltage exceeds 0.1 V, which is completely opposite to the variation tendency of current. The analysis of transmission spectra and transmission pathways reveals the physical mechanism of spin-dependent transport under high bias voltage, where the compression process induces more spin-down electron channels. Moreover, the coupling between Ni tip electrode and propynyl of P-TOTA molecule is enhanced in the compression process, which modifies the organic–ferromagnetic spinterface significantly. The results of PDOS and LDOS illuminate that orbital hybridization between 3d orbitals of Ni tip atom and 2p orbitals of C atoms of propynyl occurs at the spinterface. More importantly, the weak orbital hybridization results in strong spin-up polarized density of states, but strong orbital hybridization activates the spin-down electron transmission and leads the spin polarization to decrease. As a consequence, the orbital hybridization of organic–ferromagnetic spinterface plays a vital role in determining the spin-dependent transport properties of P-TOTA molecular junction. Our theoretical work reveals the physical mechanism of spin transport properties of P-TOTA molecular junction and promotes its application in molecular spintronic devices.

Acknowledgements

Project supported by the National Natural Science Foundation of China (Grant Nos. 11974217 and 11874242) and the Natural Science Foundation of Shandong Province, China (Grant No. ZR2018MA037).

References

[1] Naber W J M, Faez S and Wiel W G V 2007 *J. Phys. D: Appl. Phys.* **40** R205
[2] Sanvito S 2011 *Chem. Soc. Rev.* **40** 3336
[3] Lv X R, Liang S H, Tao L L and Han X F 2014 *Spin* **4** 1440013
[4] Gu X R, Guo L D and Sun X N 2018 *Chin. Phys. B* **27** 107202
[5] Hirohata A, Yamada K, Nakatani Y, Prejbeanu I L, Diény B, Pirro P and Hillebrands B 2020 *J. Magn. Magn. Mater.* **509** 166711
[6] Rocha A R, Garcia-Suarez V M, Bailey S W, Lambert C J, Ferrer J and Sanvito S 2005 *Nat. Mater.* **4** 335
[7] Sun D, Ehrenfreund E and Valy Z V 2014 *Chem. Commun.* **50** 1781
[8] Sanvito S 2010 *Nat. Phys.* **6** 562
[9] Barraud C, Seneor P, Mattana R, Fusil S, Bouzehouane K, Deranlot C, Graziosi P, Hueso L, Bergenti I, Dediu V, Petroff F and Fert A 2010 *Nat. Phys.* **6** 615
[10] Sun M and Mi W 2018 *J. Mater. Chem. C* **6** 6619
[11] Cinchetti M, Dediu V A and Hueso L E 2017 *Nat. Mater.* **16** 507
[12] Delprat S, Galbiati M, Tatay S, Quinard B, Barraud C, Petroff F, Seneor P and Mattana R 2018 *J. Phys. D: Appl. Phys.* **51** 473001
[13] Galbiati M, Tatay S, Barraud C, Dediu A V, Petroff F, Mattana R and Seneor P 2014 *MRS Bull.* **39** 602
[14] Guo L, Gu X, Zhu X and Sun X 2019 *Adv. Mater.* **31** 1805355
[15] Raman K V, Kamerbeek A M, Mukherjee A, Atodiresei N, Sen T K, Lazic P, Caciuc V, Michel R, Stalke D, Mandal S K, Blügel S, Münzenberg M and Moodera J S 2013 *Nature* **493** 509
[16] Li D and Smogunov A 2021 *Phys. Rev. B* **103** 085432
[17] Qiu S, Miao Y Y, Zhang G P, Ren J F, Wang C K and Hu G C 2020 *J. Phys. Chem. C* **124** 12144
[18] Qiu S, Miao Y Y, Zhang G P, Ren J F, Wang C K and Hu G C 2020 *J. Mater. Sci.* **55** 16311
[19] Qiu S, Miao Y Y, Zhang G P, Ren J F, Wang C K and Hu G C 2019 *J. Magn. Magn. Mater.* **479** 247
[20] Li S, Wang Y D, Wang Y F, Sanvito S and Hou S M 2021 *J. Phys. Chem. C* **125** 6945
[21] Li D, Banerjee R, Mondal S, Maliyov I, Romanova M, Dappe Y J and Smogunov A 2019 *Phys. Rev. B* **99** 115403
[22] Niu L L, Fu H Y, Suo Y Q, Liu R, Sun F, Wang S S, Zhang G P, Wang C K and Li Z L 2021 *Physica E* **128** 114542
[23] Koley S and Chakrabarti S 2017 *J. Phys. Chem. C* **121** 21695
[24] Deng Y X, Chen S Z, Zeng Y, Zhou W X and Chen K Q 2017 *Org. Electron.* **50** 184
[25] Cardona-Serra S, Gaita-Ariño A, Stamenova M and Sanvito S 2017 *J. Phys. Chem. Lett.* **8** 3056
[26] Dhungana K B and Pati R 2014 *Appl. Phys. Lett.* **104** 162404
[27] Zhao W K, Zou D Q, Yang C L and Sun Z P 2017 *J. Mater. Chem. C* **5** 8862
[28] Wang Z Q, Tang F, Dong M M, Wang M L, Hu G C, Leng J C, Wang C K and Zhang G P 2020 *Chin. Phys. B* **29** 067202
[29] Jasper-Tönnies T, Garcia-Lekue A, Frederiksen T, Ulrich S, Herges R and Berndt R 2017 *Phys. Rev. Lett.* **119** 066801
[30] Wei Z M, Wang X T, Borges A, Santella M, Li T, Sørensen J K, Vanin M, Hu W P, Liu Y Q, Ulstrup J, Solomon G C, Chi Q J, Bjørnholm T, Nørgaard K and Laursen B W 2014 *Langmuir* **30** 14868
[31] Jasper-Tönnies T, Garcia-Lekue A, Frederiksen T, Ulrich S, Herges R and Berndt R 2019 *J. Phys.: Condens. Matter* **31** 18LT01
[32] Jasper-Tönnies T, Weismann A, Frederiksen T, Garcia-Lekue A, Ulrich S, Herges R and Berndt R 2019 *Phys. Rev. B* **99** 245417
[33] Jasper-Tönnies T, Poltavsky I, Ulrich S, Moje T, Tkatchenko A, Herges R and Berndt R 2018 *J. Chem. Phys.* **149** 244705
[34] Brandbyge M, Mozos J L, Ordejón P, Taylor J and Stokbro K 2002 *Phys. Rev. B* **65** 165401
[35] José M S, Emilio A, Julian D G, Alberto G, Javier J, Pablo O and Daniel S P 2002 *J. Phys.: Condens. Matter* **14** 2745
[36] Atomistix ToolKit version 2018.06, Synopsys QuantumWise A/S (www.quantumwise.com)
[37] Perdew J P, Burke K and Ernzerhof M 1996 *Phys. Rev. Lett.* **77** 3865
[38] Troullier N and Martins J 1990 *Solid State Commun.* **74** 613
[39] Liu R, Bi J J, Xie Z, Yin K, Wang D, Zhang G P, Xiang D, Wang C K and Li Z L 2018 *Phys. Rev. Appl.* **9** 54023
[40] Li Z L, Bi J J, Liu R, Yi X H, Fu H Y, Sun F, Wei M Z and Wang C K 2017 *Chin. Phys. B* **26** 098508
[41] Landauer R 1970 *Philos. Mag.* **21** 863
[42] Larade B, Taylor J, Zheng Q R, Mehrez H, Pomorski P and Guo H 2001 *Phys. Rev. B* **64** 195402